

LASERS

https://doi.org/10.1070/QEL16287

Single-walled carbon nanotube tunable mode-locked soliton fibre laser

H. Ahmad, S.A. Reduan, M.F. Ismail, K. Thambiratnam

Abstract. **A soliton fibre laser with a tunable mode-locked output is proposed and demonstrated. The laser is based on a conventional erbium-doped fibre and uses single-walled carbon nanotubes (SWCNTs) as a saturable absorber (SA). Tuning is performed using a tunable Mach–Zehnder filter (TMZF). The SWCNT-based SA has a modulation depth of ~19.0% and saturation intensity of 45.3 MW cm^{-2}. Mode-locking begins at a pump power of 6.0 mW and allows pulsed outputs to be generated from 1550 nm to 1566 nm. The 3 dB bandwidth and pulse duration of the output pulse vary slightly from 6.34 nm to 6.90 nm and from 0.51 ps to 0.56 ps, respectively, which results in the corresponding time-bandwidth product varying from 0.40 to 0.46. The results suggest that the proposed laser would have significance advantages in many applications, particularly spectroscopy and telecommunications.**

Keywords: *fibre laser, Q-switching, single-walled nanotube, saturable absorber, S-band, tunable laser, pulsed laser, erbium-doped fibre.*

1. Introduction

Tunable passively mode-locked fibre lasers are very attractive for scientific and industrial applications such as materials processing, telecommunications, spectroscopy and biomedical research [1–6]. Due to their compactness, simplicity and cost-effectiveness [1, 7–9], a fibre laser with a passively mode-locked output is preferable in comparison with a similar actively mode-locked system requiring additional switching electronics [10]. Passive mode-locking is typically provided by integrating a nonlinear optical device, known as saturable absorber (SA), into the laser cavity.

In the drive towards developing SAs for use in laser cavities, semiconductor SA mirrors (SESAMs) have become one of the first commercial SAs that were used for the generation of pulsed laser outputs. This was due to their excellent performance, which in turn was a product of well-developed semiconductor technologies [11]. However, the inherent limitations of SESAMs soon became apparent: They proved to be extremely complex to fabricate and required highly specialised equipment, as well as were costly, bulky and complex to operate in fibre applications [12, 13]. This quickly resulted in other potential SA technologies being explored, and a new candidate was found in the form of single-wall carbon nanotubes (SWCNTs). SAs based on SWCNTs were simple and cheap to fabricate [14] and possessed highly desirable optical characteristics such as subpicosecond recovery time, low saturation intensity and ultrafast response time of less than 1 ps as well as mechanical robustness [12, 15–19], leading them to become the preferred choice for use as an SA.

Subsequently, SWCNTs have found multiple applications as SAs for the generation of ultrafast pulses from fibre laser systems. Most recently, a tunable mode-locked fibre laser using SWCNT-based SAs has been demonstrated [3, 20, 21] using tunable band pass filters (TBPFs), fibre taper filters and polarisation controllers to ensure wavelength tuning. However, the use of these devices in a soliton mode-locked fibre laser would eventually suppress or eliminate the Kelly sidebands because of the spectral confinement effect of these devices [3, 22]. Ahmad et. al. reported the successful use of a tunable Mach–Zehnder filter (TMZF) [23] in a graphene-based mode-locked fibre laser, proving that the TMZF is a highly suitable tuning mechanism for mode-locked fibre lasers, in particular for soliton mode-locked fibre lasers.

In this work, a tunable mode-locked fibre laser utilising a SWCNT-based SA as the pulse inducing mechanism and a TMZF as the wavelength tuning mechanism is proposed and demonstrated. The proposed laser is capable of providing a tuning range of approximately 16 nm, with output pulses that have a repetition rate of 12.7 MHz and correspond to a period of 78.7 ns at a pump power of 6.0 mW. The 3 dB bandwidth and pulse duration of the output pulses varies slightly from 6.24 to 6.90 nm and 0.51 to 0.56 ps, respectively, while the time bandwidth product (TBP) varies from 0.40 to 0.46. The proposed system is capable of successfully conserving the Kelly sidebands of the soliton spectrum using the TMZF as a tunability filter device. This is also the first time, to the best knowledge of the authors, that an SWCNT-based tunable mode-locked fibre laser using a TMZF as the tuning mechanism has been reported and demonstrated.

2. Experiment setup

2.1. Fibre laser

Figure 1 shows the schematic of the proposed tunable mode-locked soliton fibre laser in a ring configuration. The laser cavity consists of a 3-m-long M-12 980/125 erbium-doped fibre (EDF) produced by Fibrecore Inc., which has a cut-off wavelength of 911 nm and a numerical aperture of 0.21. The

S.A. Reduan, M.F. Ismail, K. Thambiratnam Photonics Research Center, University of Malaya, Kuala Lumpur 50603, Malaysia;
H. Ahmad Photonics Research Center, University of Malaya, Kuala Lumpur 50603, Malaysia; Department of Physics, Faculty of Science and Technology, Airlangga University, Surabaya 60115, Indonesia;
e-mail: harith@um.edu.my

Received 17 January 2018; revision received 17 February 2018
Kvantovaya Elektronika **48** (10) 930–935 (2018)
Submitted in English

EDF acts as a gain medium of the laser, and is pumped by a 974-nm laser diode (LD) through the 980 nm port of a 980/1550-nm fused wavelength division multiplexer (WDM). An isolator (ISO) is connected after the EDF to ensure unidirectional light propagation in the cavity, and is subsequently connected to a 95/5 output coupler. The 5% port captures a portion of the output signal for its subsequent analysis, where the 95% port returns light back into the cavity, which is connected to the SA, which is formed by sandwiching SWCNTs between fibre ferrules as shown in the inset of Fig. 1.

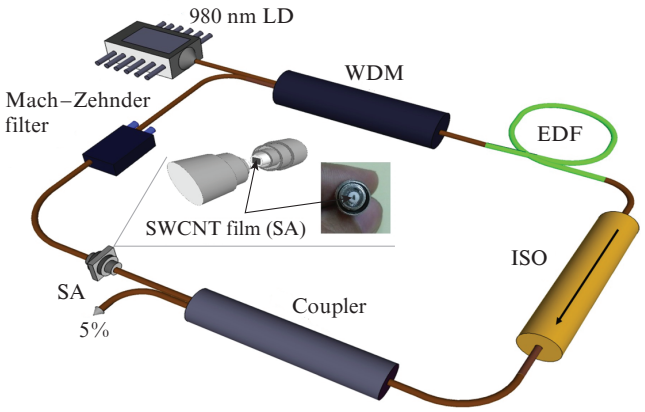

Figure 1. Experimental setup for the proposed laser.

The SWCNT film used in this work was fabricated and prepared at the Centre for Advanced Photonics and Electronics (CAPE), Cambridge University, United Kingdom, and then was embedded into a polyvinyl alcohol polymer to make a thin-film SA. The other end of the SA is connected to the TMZF, and its output is connected to the 1550-nm port of the WDM, thus completing the laser cavity. The laser cavity has a total length of about 15.7 m, with 3-m length of the EDF and 12.7-m length of a single-mode fibre (SMF), which have an estimated group velocity dispersion (GVD) of +23.2 $ps^2\ km^{-1}$ [24, 25] and –23.3 $ps^2\ km^{-1}$, respectively at 1550 nm (Table 1).

Table 1. Numerical estimation of GVD for optical fibres utilised in the proposed experiment.

Fibre type	Fibre length/m	D /ps nm^{-1} km^{-1}	λ/nm	GVD /ps^2 km^{-1}
Single-mode fibre	12.7	18	1550	–23.3
EDF	3	–18		+23.2

The GVD of the total cavity is –0.2261 ps^2, which contributes to anomalous dispersion laser operation and thus resulting in a soliton fibre laser.

A Yokogawa model AQ6370C optical spectrum analyser (OSA) is used to monitor and measure the output spectrum of the soliton fibre laser, and an Alnair HAC-200 autorcorrelator is used to measure the time properties of the mode-locked laser pulses. The characteristics of the mode-locked pulse train are measured by using a Yokogawa DLM2054 oscilloscope combined with a 1.2-GHz photodetector. The signal-to noise (SNR) ratio of the generated mode-locked pulses is measured using an Anritsu MS2683A radio-frequency spectrum analyser (RFSA).

2.2. TMZF characterisation

The Mach–Zehnder filter operation is based on the interference of two coherent monochromatic sources that are affected by the length difference and eventually the phase difference between the two arms of the filter [26, 27] (Fig. 2). It can be seen from Fig. 2 that before entering into a waveguide the optical power at the input is equally split (by directional coupler 1) between the two arms of the Mach–Zehnder filter having a length difference of ΔL. The light combines (by directional coupler 2) at different phases, for which each wave-

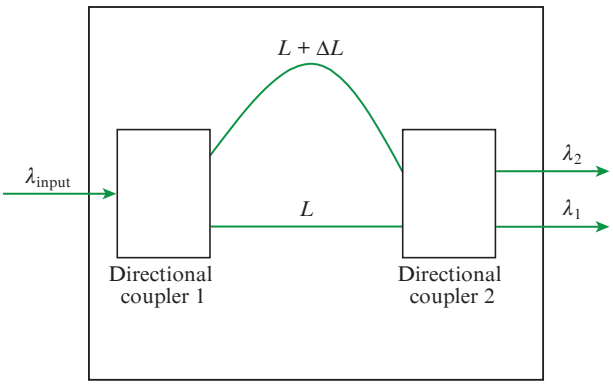

Figure 2. Operation principle of the tunable Mach–Zehnder filter.

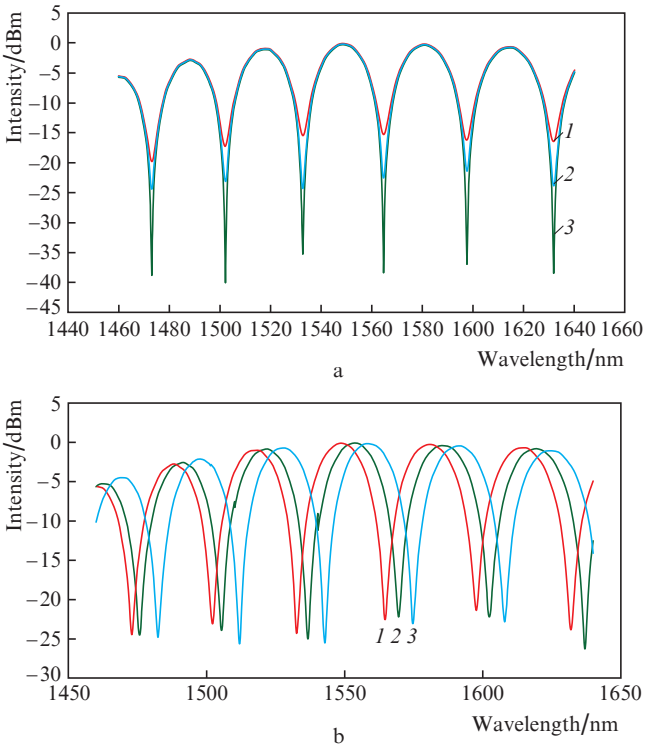

Figure 3. Output spectrum of the TMZF obtained by adjusting (a) the extinction ratio and (b) the wavelength on the filter.

length interferes constructively on one of the two output ports and destructively on the other depending on the phase variation and the position of the output fibre [26, 27]. Thus, by adjusting the quantity of ΔL, the Mach–Zhender filter can be tuned to obtain the desired phase shift at the output port. Therefore, by controlling the propagation delay of the path $L + \Delta L$ with respect to the path L we can control the phase shift. The characteristics of the TMZF used in this experiment are shown in Fig. 3.

Characterisation of the TMZF is done by adjusting the wavelength and extinction ratio, as reported by Ahmad et al. [23]. Figure 3a shows the output spectrum obtained for the characterisation of the extinction ratio tuning mechanism of the TMZF. One can see that the upper, shallow part becomes deeper as the extinction ratio is increased [curves (*2*) and (*3*)]. A tunable light source (TLS) is used to launch the signal into the TMZF for its characterisation, and the output spectrum is measured using the OSA.

It follows from Fig. 3b that the output spectrum of the TMZF consists of many peaks. Curves (*2*) and (*3*) result from the tuning of the average wavelength [curve (*1*)] of the TMZF.

3. Results and discussion

3.1. Characterisation of nanotubes

A Renishaw Raman spectroscope was used to characterise the SWCNT-based SA, with the resulting Raman spectrum shown in Fig. 4. The G peak is observed at 1593.57 cm^{-1} and indicates the presence of the carbon nanotubes in the sample being analysed. This spectrum is comparable to that reported in Refs [28–30], which agreed on the existence of the G peak at this wavelength for SWCNTs. However, distinct peak features in the spectrum can also be observed using higher excitation wavelengths, such as $\lambda = 633$ nm or 785 nm [14, 31].

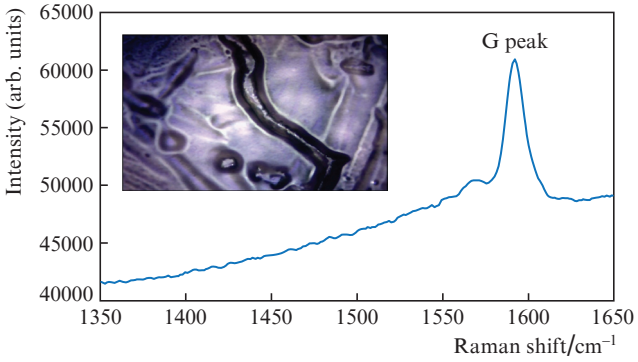

Figure 4. Raman spectrum of the SWNT film and the Raman microscope image of the SA (inset) with the excitation wavelength of 532 nm.

Figure 5a shows the linear optical absorption of the SWCNT-based SA as a function of wavelength from 900 nm to 1600 nm using white light as a signal source. One can see that the peak absorption wavelength of the SWCNT-based SA covers the C band region at the 1.5-μm wavelength range. This is highly relevant, as it is located within the erbium gain region, thus enabling the proposed laser to function optimally. Figure 5b, on the other hand, shows the nonlinear optical absorption measurement of the SWCNT-based SA.

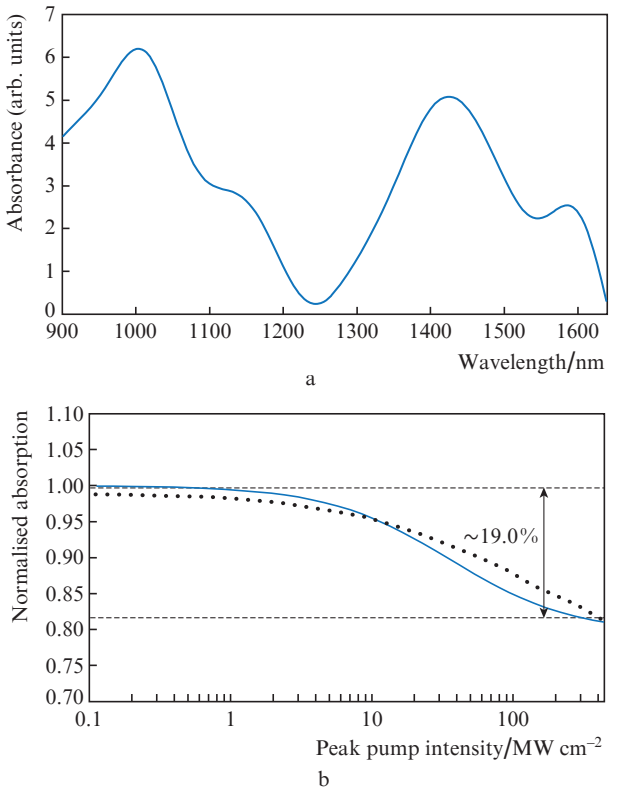

Figure 5. Optical characteristics of the SWNT film: (a) linear absorption and (b) nonlinear absorption of the SWNT film as a function of pump peak intensity (points show the experimental data and the solid curve is the result of fitting).

For this measurement, the twin-detector method is applied to characterise the optical nonlinearity of the SA, and uses a mode-locked seed laser with a centre wavelength of 1560 nm [32]. The mode-locked pulses have a repetition rate of 27.78 MHz and pulse duration of 0.74 ps.

The normalised collected data are then fitted using the saturation model formula [3, 32]:

$$\alpha(I) = \frac{\alpha_s}{1 + I/I_s} + \alpha_{ns}, \tag{1}$$

where $\alpha(I)$ is the intensity-dependent absorption; I is input intensity; I_s is saturation intensity; and α_s and α_{ns} are saturable and nonsaturable absorption, respectively. From the measurement, the saturable absorption (modulation depth) and saturation intensity are ~19.0% and 45.3 MW cm^{-2}, respectively. These values of SWNTs are comparable with those reported by Sun et al. [28] and Chiu et al. [33]. The characterisation of the SWCNT samples makes it possible to conclude that the modulation depth and saturation intensity of the fabricated SA is sufficient for pulse shaping and stabilising the generated pulses [34].

3.2. Tunable mode-locked pulse output with the TMZF

In the operation of the proposed tunable mode-locked fibre laser, continuous wave lasing begins at a threshold pump power of 4.5 mW, whereas the threshold pump power for self-started mode-locked operation is 6.0 mW. The observed output optical spectrum shows sidebands which confirm that the

pulsed laser operated in the soliton regime. The tuning range in this experiment is 16 nm, covering a centre wavelength from 1550 nm to 1566 nm by simultaneously adjusting the extinction ratio and wavelength of the TMZF as shown in Fig. 6. It is observed that the Kelly sidebands are visible and conserved as the centre wavelength is tuned. However, mode-locked operation dissipates as the centre wavelength moves beyond 1566 nm at a threshold pump power of 6.0 mW. However, increasing the pump power will result in mode-locked operation restarting by the reappearance of the soliton spectrum at centre wavelengths higher than 1566 nm, at approximately 1567, 1568 and 1569 nm. This behaviour is attributed to the gain of the EDF; as the centre wavelength moves beyond the optimal gain region of the active fibre, the gain drops, and thus lasing becomes unstable. However, increasing the pump power imparts more gain at the longer wavelength regions, thus allowing for a wider mode-locked tuning range.

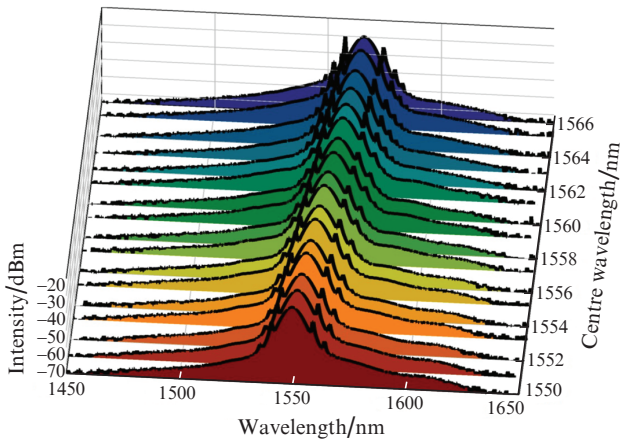

Figure 6. Output spectra of the tunable mode-locked laser for 17 different centre wavelength with the Kelly sidebands being conserved.

Figure 7 displays the output spectrum of different wavelengths at a constant pump power of 7.0 mW. The TMZF characterisation shows an insignificant loss in intensity of the filter for a wavelength higher than 1560 nm as expected. This phenomenon is believed to prevent mode-locked operation at wavelengths beyond 1566 nm. Thus, it can be concluded that the gain profile of the active fibre is the limiting factor rather than the SWCNT-based SA. The performance of the system can be further enhanced by using a low loss tunable filter to tune the centre wavelength for a broader range.

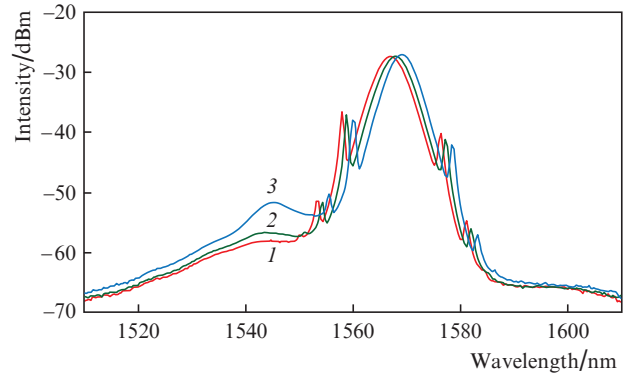

Figure 7. Output spectra of the tunable mode-locked laser for centre wavelengths of (*1*) 1567, (*2*) 1568 and (*3*) 1569 nm at a pump power of 7.0 mW.

Autocorrelation traces for the 17 different centre wavelengths are shown in Fig. 8. By assuming a sech^2 pulse shape for anomalous dispersion, the estimated pulse duration at full-width at half maximum (FWHM) varies between 0.51 to 0.56 ps.

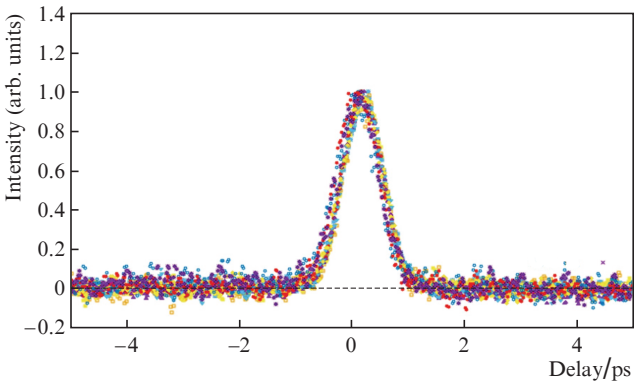

Figure 8. Autocorrelator traces of the mode-locked pulsed laser for 17 different centre wavelengths ranging from 1550 to 1566 nm.

Figure 9 shows the 3-dB bandwidth, pulse duration and corresponding time bandwidth product (TBP) of 17 different centre wavelengths as functions of wavelength. The values of 3-dB bandwidth vary slightly from 6.24 to 6.90 nm. The pulse duration and TBP values shows significantly less variance between 0.51 to 0.56 ps and 0.40 to 0.46, respectively. The TBP values exhibit only a significantly less variance over the wavelength range, indicating the fact that the generated pulses are in fact soliton-like pulses. The TBP values are higher than the values of transform-limited sech^2 pulses (TBP = 0.315) [27], indicating that the pulses exhibit a chirping effect [35].

The pulse train waveform of the tunable mode-locked laser as observed from the oscilloscope is shown in Fig. 10. The repetition rate of the mode-locked laser pulses is 12.7 MHz, corresponding to a 78.7-ns period in the pulses within the time domain. The repetition rate obtained from the proposed system is larger than that previously reported in a graphene-

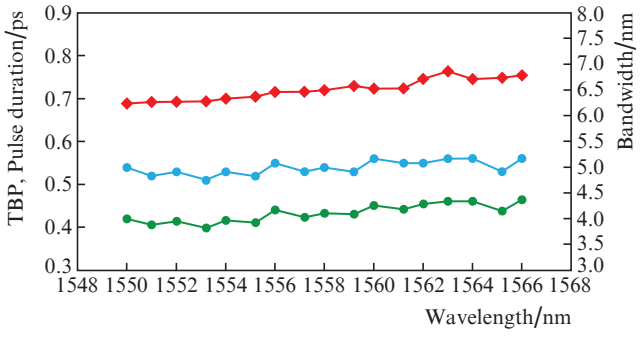

Figure 9. (●) Time bandwidth product, (●) pulse duration and (◆) bandwidth at a level of 3 dB as functions of the centre wavelength.

based tunable mode-locked laser [23]. The repetition rate of mode-locked pulses depends on the cavity length; thus, a longer cavity length produces a lower repetition rate and vice-versa:

$$f_r = c/(nL), \quad (2)$$

where f_r is the repetition rate; c is the velocity of light in vacuum and ($\sim 3 \times 10^8$ m s^{-1}); and n is the refractive index of the cavity, which is approximately 1.5. The pulse energy of the mode-locked pulses is measured to be about 2 pJ.

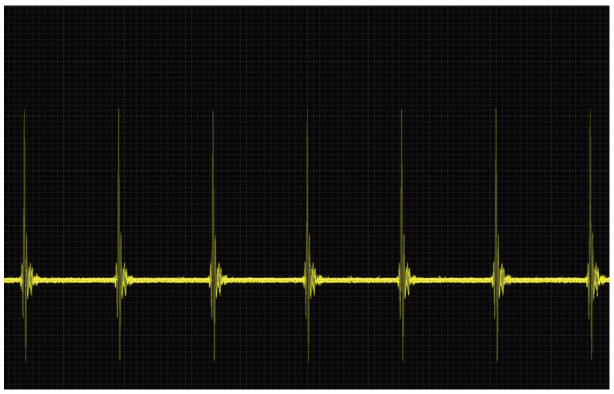

Figure 10. Oscilloscope waveform of the pulse train of the tunable mode-locked laser.

It follows from Fig. 11 that the SNR ratio of the mode-locked operation at a fundamental frequency of 12.7 MHz is about 60 dB. The inset of Fig. 11 shows the RF spectrum in a wider span, implying the typical characteristics of a mode-locked pulse output [36–39]. The measured SNR indicates that the mode locked pulsed laser is highly stable, with low amplitude noise fluctuations and low time jitter [28, 40].

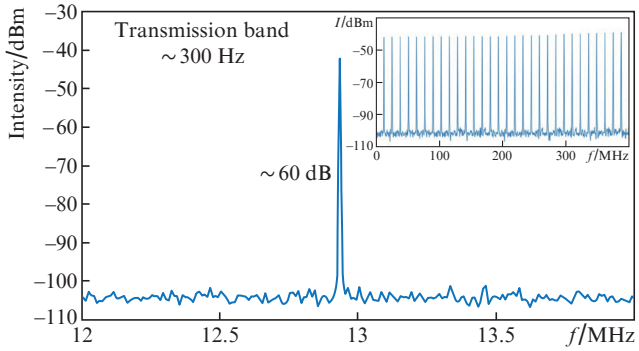

Figure 11. Radio-frequency optical spectrum at the fundamental frequency (f = 12.7 MHz) and the wideband RF spectrum (inset).

The proposed laser is capable of generating tunable mode-locked pulses with a repetition rate of 12.7 MHz at a low pump power of 6.0 mW, compared to that previously reported in a graphene tunable mode-locked fibre laser [23]. Furthermore, the proposed SWCNT-based tunable mode-locked pulsed fibre laser is capable of providing lower deviations in its tuning range by ~1 nm, with Kelly sidebands conserved [3]. The proposed laser can find numerous applications that require stable pulse operation with a wide tunability wavelength range at low pump powers.

4. Conclusions

A tunable mode-locked, soliton fibre laser using a SWCNT-based SA and a TMZF as the tuning mechanism is proposed and demonstrated. Soliton mode-locked pulses are generated at a pump power of 6.0 mW in a wavelength range between 1550 nm to 1566 m with a deviations of ~1 nm. The SA has a modulation depth and saturation intensity of ~19.0% and 45.3 MW cm^{-2}, respectively. The 3-dB bandwidth and pulse duration of the laser output varies from 6.24 to 6.90 nm and from 0.51 ps to 0.56 ps, respectively. The corresponding TBP also varies slightly from 0.40 to 0.46 for different centre wavelengths. The proposed laser is highly suitable for various applications in such fields as spectroscopy, telecommunication, sensing and biomedical research.

Acknowledgements. The authors would like to thank the Ministry of Higher Education (MOHE), Malaysia, and the University of Malaya for providing financial support for this work under [Grants LRGS (2015) NGOD/UM/KPT, GA 010 – 2014 (ULUNG), RU001-2017 and BR003 – 2016].

References

1. Okhotnikov O., Grudinin A., Pessa M. *New J. Phys.*, **6** (1), 177 (2004).
2. Letokhov V. *Nature*, **316**, 325 (1985).
3. Wang F., Rozhin A., Scardaci V., Sun Z., Hennrich F., White I., et al. *Nature Nanotechnology*, **3** (12), 738 (2008).
4. Sun Z., Popa D., Hasan T., Torrisi F., Wang F., Kelleher E.J., et al. *Nano Research*, **3** (9), 653 (2010).
5. Marshall J., Stewart G., Whitenett G. *Measurement Science and Technology*, **17** (5), 1023 (2006).
6. Zhang H., Tang D., Zhao L., Bao Q., Loh K.P., Lin B., et al. *Laser Phys. Lett.*, **7** (8), 591 (2010).
7. Nelson L., Jones D., Tamura K., Haus H., Ippen E. *Appl. Phys. B*, **65** (2), 277 (1997).
8. Fermann M., Galvanauskas A., Sucha G., Harter D. *Appl. Phys. B*, **65** (2), 259 (1997).
9. Cao W., Wang H., Luo A., Luo Z., Xu W. *Laser Phys. Lett.*, **9** (1), 54 (2011).
10. Svelto O. *Principles of Lasers* (Berlin-Heidelberg: Springer, 2010).
11. Keller U. *Nature*, **424**, 831 (2003).
12. Martinez A., Sun Z. *Nature Photon.*, **7** (11), 842 (2013).
13. Sotor J., Sobon G., Macherzynski W., Abramski K. *Laser Phys. Lett.*, **11** (5), 055102 (2014).
14. Sun Z., Hasan T., Ferrari A. *Phys. E: Low-dimensional Systems and Nanostructures*, **44** (6), 1082 (2012).
15. Set S.Y., Yaguchi H., Tanaka Y., Jablonski M. *IEEE J. Sel. Top. Quantum Electron.*, **10** (1), 137 (2004).
16. Della Valle G., Osellame R., Galzerano G., Chiodo N., Cerullo G., Laporta P., et al. *Appl. Phys. Lett.*, **89** (23), 231115 (2006).
17. Rozhin A., Scardaci V., Wang F., Hennrich F., White I., Milne W., et al. *Phys. Stat. Solidi (b)*, **243** (13), 3551 (2006).
18. Nicholson J., Windeler R., DiGiovanni D. *Opt. Express*, **15** (15), 9176 (2007).
19. Travers J., Morgenweg J., Obraztsova E., Chernov A., Kelleher E., Popov S. *Laser Phys. Lett.*, **8** (2), 144 (2011).
20. Fang Q., Kieu K., Peyghambarian N. *IEEE Photon. Technol. Lett.*, **22** (22), 1656 (2010).
21. Chamorovskiy A.Y., Marakulin A., Kurkov A., Okhotnikov O. *Laser Phys. Lett.*, **9** (8), 602 (2012).

22. Tamura K., Doerr C., Haus H., Ippen E. *IEEE Photon. Technol. Lett.*, **6** (6), 697 (1994).
23. Ahmad H., Muhammad F., Zulkifli M., Harun S. *IEEE Photon. J.*, **5** (5), 1501709 (2013).
24. Gerlein F., Cloutier S.G., in *Frontiers Optics 2010/Laser Science XXVI* (OSA, 2010) FTuJ4.
25. Sun Z., Mou C., Song Y., Yan Z., Zhou K., Zhang L., in *Advanced Photonics* (OSA, 2014) paper BW3D.4.
26. Djordjevic I., Ryan W., Vasic B. *Fundamentals of Optical Communication. Coding for Optical Channels* (Berlin-Heidelberg: Springer, 2010) pp. 25–73.
27. Agrawal G. *Applications of Nonlinear Fiber Optics* (New York: Academic Press, 2001).
28. Sun Z., Hasan T., Wang F., Rozhin A.G., White I.H., Ferrari A.C. *Nano Research*, **3** (6), 404 (2010).
29. Kim S.-J., Park J., Jeong Y., Go H., Lee K., Hong S., et al. *Nanoscale Res. Lett.*, **9** (1), 1 (2014).
30. Gaufrès E., Tang N.-W., Lapointe F., Cabana J., Nadon M.-A., Cottenye N., et al. *Nature Photon.*, **8** (1), 72 (2014).
31. Hasan T., Sun Z., Wang F., Bonaccorso F., Tan P.H., Rozhin A.G., et al. *Adv. Mater.*, **21** (38–39), 3874 (2009).
32. Ahmad H., Reduan S., Ali Z.A., Ismail M., Ruslan N., Lee C., et al. *IEEE Photon. J.*, **8** (1), 1 (2016).
33. Chiu J.-C., Lan Y.-F., Chang C.-M., Chen X.-Z., Yeh C.-Y., Lee C.-K., et al. *Opt. Express*, **18** (4), 3592 (2010).
34. Keller U. *Progress Opt.*, **46**, 1 (2004).
35. Set S.Y., Yaguchi H., Tanaka Y., Jablonski M. *J. Lightwave Technol.*, **22** (1), 51 (2004).
36. Dou Z., Song Y., Tian J., Liu J., Yu Z., Fang X. *Opt. Express*, **22** (20), 24055 (2014).
37. Yin K., Zhang B., Li L., Jiang T., Zhou X., Hou J. *Photon. Research*, **3** (3), 72 (2015).
38. Luo Z., Li Y., Zhong M., Huang Y., Wan X., Peng J., et al. *Photon. Research*, **3** (3), A79 (2015).
39. Li X., Yu X., Sun Z., Yan Z., Sun B., Cheng Y., et al. *Sci. Rep.*, **5**, 16624 (2015).
40. Von der Linde D. *Appl. Phys. B*, **39** (4), 201 (1986).